Development 121, 2005-2018 (1995)
Printed in Great Britain © The Company of Biologists Limited 1995

How do sea urchins invaginate? Using biomechanics to distinguish between mechanisms of primary invagination

Lance A. Davidson[1], M. A. R. Koehl[2], Raymond Keller[3] and George F. Oster[3]

[1]Graduate Group in Biophysics, 201 Wellman Hall, University of California at Berkeley, Berkeley, CA 94720, USA
[2]Department of Integrative Biology, Valley Life Sciences Building, University of California at Berkeley, Berkeley, CA 94720, USA
[3]Department of Molecular and Cell Biology, Division of Cell and Developmental Biology, Life Sciences Addition, University of California at Berkeley, Berkeley, CA 94720, USA

SUMMARY

The forces that drive sea urchin primary invagination remain mysterious. To solve this mystery we have developed a set of finite element simulations that test five hypothesized mechanisms. Our models show that each of these mechanisms can generate an invagination; however, the mechanical properties of an epithelial sheet required for proper invagination are different for each mechanism. For example, we find that the gel swelling hypothesis of Lane et al. (Lane, M. C., Koehl, M. A. R., Wilt, F. and Keller, R. (1993) *Development* 117, 1049-1060) requires the embryo to possess a mechanically stiff apical extracellular matrix and highly deformable cells, whereas a hypothesis based on apical constriction of the epithelial cells requires a more compliant extracellular matrix. For each mechanism, we have mapped out a range of embryo designs that work. Additionally, the simulations predict specific cell shape changes accompanying each mechanism. This allows us to design experiments that can distinguish between different mechanisms, all of which can, in principle, drive primary invagination.

Key words: gastrulation, invagination, epithelial buckling, apical constriction, gel swelling, cell tractoring, apicobasal contraction, finite element methods, biomechanics, sea urchin

INTRODUCTION

Primary invagination in the sea urchin begins when the flattened epithelial sheet of the vegetal plate bends inwards to form the archenteron. Primary invagination ends and secondary invagination begins when the mesenchyme cells at the tip of the archenteron send out filopodia and the archenteron extends to cross the remainder of the blastocoel. Any explanation of how primary invagination works must incorporate both the passive mechanical properties of the embryo as well as the force-generating mechanisms within the epithelial sheet driving invagination.

A century of research on primary invagination has spawned many hypotheses, some of which are summarized in Table 1 (e.g. Gustafson and Wolpert, 1963; Ettensohn, 1985; Hardin, 1987b; Nislow and Morrill, 1988; Bard, 1990; Burke et al., 1991; Lane et al., 1993; Hardin, 1994).

His (1874) proposed that 'proliferative pressure' due to cell division drove invagination. One interpretation of this idea is that cell division in the central region of the vegetal plate pushes against cells in the periphery (Trinkaus, 1984); if the peripheral tissue resists being stretched, the expanding central tissue of the vegetal plate will be compressed and buckle. Although increases in cell division have been observed in the vegetal half during primary invagination (Nislow and Morrill, 1988), treatment of embryos with a DNA synthesis inhibitor, aphidicolin, demonstrated that cell division is not necessary for invagination (Stephens et al., 1986).

Rhumbler (1902) proposed that a decrease in the hydrostatic pressure of the blastocoel buckled the vegetal plate. However, this was ruled out by Moore and Burt (1939), who found that vegetal plates dissected from early gastrulae would invaginate without an intact blastocoel. Later, Ettensohn (1984a) demonstrated the same phenomenon in late mesenchyme blastulae. These microdissection studies showed that the forces responsible for invagination must reside in the vegetal plate itself.

Gustafson and Wolpert (1963) proposed an hypothesis based on differential cell adhesion. They observed that cells in the center of the vegetal plate reduce their intercellular contacts and round-up on their basal surfaces. This led them to propose that the apical ends of these cells maintain strong attachments to the ECM; reduced cell-cell adhesion would lead to expansion of the basal ends of the cells relative to their apical ends. If the cell sheet lateral to the vegetal plate provides a stiff foundation that resists being stretched, the center of the expanding vegetal plate will be compressed and buckle inward to form the archenteron. This hypothesis has proved difficult to test since changes in apparent intercellular contact in the vegetal plate may arise either from adhesive forces, or from forces generated parallel to the apicobasal axis within the lateral cell cortex (Gustafson and Wolpert, 1963; Clausi and Brodland, 1993).

Because of the conclusive evidence against the blastocoel hydrostatic pressure and the cell division hypotheses, only five hypotheses (Table 1) will be investigated in this paper: (i)

Table 1. Hypotheses for the mechanism driving primary invagination in sea urchin

Proposal	Supporting evidence	Evidence against
Apical constriction of cells in the vegetal plate causes movement of cytoplasm from apical to basal ends of cells, resulting in an invagination.	Microfilaments observed arranged in a sub–apical cortex of vegetal plate cells of mesenchyme blastula (Anstrom, 1992) and early gastrula (Ettensohn, 1984a).	No clear decrease in the apical surface area of the vegetal plate cells (Ettensohn, 1984b). Cytochalasin D treatment does not block gastrulation (Lane et al., 1993).
Cell tractoring of cells lateral to the vegetal plate toward the center of the vegetal plate causes buckling.	Marked vegetal cells move toward the vegetal plate during invagination. Observed protrusions and cell shapes in vegetal cells skewed toward the center of the vegetal plate (Burke et al., 1991).	[none]
Contraction of a contiguous microfilament ring surrounding the vegetal plate causes buckling.	Observations of skewed cell shapes lateral to the center of the vegetal plate (Ettensohn, 1984a; Burke et al., 1991).	[none]
Apicobasal contraction of sub-cortical cytoskeletal structures generating compression within cells of the vegetal plate causes buckling.	Observations of decreases of lateral membrane shared between cells of the vegetal plate (Gustafson and Wolpert, 1963).	Only a 15% decrease in cell height seen for cells within the vegetal plate (Ettensohn, 1984b).
Regulated secretion of a hydrophilic chondroitin sulfate proteoglycan swells the apical lamina and buckles the vegetal plate.	Stimulation of secretion with the Ca^{2+} ionophore A23187 causes premature invagination. An inhibitor of secretion, monensin, blocks invagination (Lane et al., 1993).	[none]

apical constriction of vegetal plate cells (Lewis, 1947), (ii) cell tractoring of cells lateral to the vegetal plate (Burke et al., 1991), (iii) contraction of a cytoskeletal bundle running in a ring through the apical edge of a circle of cells surrounding the vegetal plate (Martin and Lewis, 1992), (iv) apicobasally aligned contraction of the cell cortex of cells within the vegetal plate (proposed by Gustafson and Wolpert (1963) as a corollary to the differential adhesion hypothesis), and (v) swelling of a polyelectrolyte gel secreted by vegetal plate cells into the apical ECM (Lane et al., 1993). We test the apicobasal contraction hypothesis because it is a mechanically relevant consequence of the differential adhesion hypothesis, which we cannot test directly with our methods. Each of these hypotheses will be described below.

To investigate these five hypothesized mechanisms of primary invagination, we will proceed by formulating a general biomechanical model to calculate the early movements of primary invagination produced by each mechanism. The model allows us to predict the cell shape changes within the vegetal plate produced by each mechanism, and to determine the relative stiffnesses of the cell and ECM layers required by each mechanism to produce an invagination. Finally, we list the mechanical parameters that must be measured, and/or manipulated, in order to test each of these proposed mechanisms for primary invagination.

Mechanical models for epithelial buckling

Invagination is the direct consequence of a pattern of forces exerted by cells and extracellular matrix (ECM) on the vegetal plate causing it to bend inward. A material's elastic modulus, or stiffness, characterizes its resistance to deformation when subjected to stress. Stress is force per cross-sectional area of the material bearing that force. Forces acting on tissues with low elastic modulii will produce larger strains than the same forces acting on tissues with high elastic modulii. Strain is a dimensionless deformation, such as a change in length divided by the undeformed length. A review of biomechanics as it applies to embryonic tissues can be found in Koehl (1990) and Brodland (1994). Although a few empirical studies of embryo mechanics have been done (e.g. Waddington 1939, 1942; Moore 1941; Selman 1955, 1958; Adams et al. 1990; Koehl et al. 1990), experiments with physical analogs and computer simulations have been the principle tools used to investigate the role of mechanics in morphogenesis.

In the early half of this century, physical simulations were used to explore epithelial bending mechanics. Butschli (1915) used spring steel and wire to reproduce the overall form of a buckling epithelium. Spek (1918) fashioned embryonic forms out of gelatin and subjected them to various salts and osmotic conditions inducing shapes that resembled *Amphioxus* gastrulae. Lewis (1947) developed mechanical models to test whether apical contraction could drive epithelial invagination. He used brass bars to represent shared cell-cell boundaries, and rubber bands to mimic the apical and basal faces of the epithelium. These mechanical epithelia buckled if there was a difference in tension between the two faces.

Physical simulations proved useful in testing the plausibility of various mechanical mechanisms, but the difficulty of constructing models and of scaling the mechanical properties correctly limited their utility (Goodier and Thomson, 1944; Baker et al., 1973). Therefore, computational models of epithelial buckling have largely replaced physical models. For instance, in a computer simulation that was similar to the physical constructs of Lewis, Odell et al. (1981) combined the

mechanism of apical contraction with a hypothetical mechanochemical trigger mechanism for propagating the contraction signal. By installing the force-generating mechanism of apical contraction into a variety of physical structures, they demonstrated that apical contraction could account for amphibian neurulation, furrow formation in *Drosophila*, and primary invagination in the sea urchin. Dunnett et al. (1991) extended this approach to a more detailed analysis of neurulation. Clausi and Brodland (1993) used a finite element model to demonstrate a role for circumferential microfilament bundles in amphibian neurulation. Cheng developed a finite element model to characterize the effects of bending forces on thin shell structures and used this model to simulate secondary invagination in the sea urchin (Hardin and Cheng, 1986; Cheng, 1987a,b). Hardin and Keller (1988) also used this modeling approach to investigate the role of bending moments generated by bottle cells during the initiation of blastopore formation in *Xenopus*. These simulations and physical models have demonstrated that several force-generating mechanisms can serve to drive the invagination of an epithelial sheet.

Finite element modeling

The finite element method (FEM) is a numerical approach to solving complicated problems in the mechanics of structures that defy solution by classical analytical and numerical methods (e.g. Zienkiewicz and Taylor, 1989, 1991; Brodland, 1994). The key to this method is to divide the structure into a series of subunits (*finite elements*). A complex structure may be divided into hundreds or thousands of finite elements. The size and shape of an individual finite element represents a block of material and does not necessarily represent a cell. Each finite element has a simple geometry which permits a simple solution for its deformation. The deformation of a structure subjected to a set of forces is obtained by numerically assembling the deformations of all the finite elements.

FEM is a common tool in engineering, and its use is also widespread in biomechanical analyses of the growth and remodeling of skeletal structures, including mammalian bones (Carter, 1987; Carter et al., 1991) and sea urchin tests (Baron, 1991). However, FEM models have been used in only a few studies of early morphogenesis (Cheng, 1987a,b; Selker et al., 1992; Clausi and Brodland, 1993). Advances in commercially available finite element codes (Mills, 1991) and the widespread availability of high speed computer workstations now make it possible to address biomechanical problems as complex as invagination.

MATERIALS AND METHODS

Computer and software

We have chosen the commercial finite element analysis program NASTRANS (MacNeal-Schwendler Corporation, Los Angeles CA) for our simulations. This program has been designed to handle large deformations of complex structures incorporating time-dependent material properties. All simulations were run on a Sun Microsystems Corporation SparcStation 10 running SunOS 4.1.3, and input files for each are available on request.

To reduce the computation time for each simulation, we assume the embryo is rotationally symmetric so that we need model only one quarter of the vegetal half of the embryo. We placed boundary conditions along longitudinal edges to emulate the presence of the other three quarters of the vegetal plate. This allowed the modeled quarter to move along these longitudinal boundaries as if attached to a mirror image of itself. Additional boundary conditions were placed to emulate the animal half of the embryo.

Embryo culture

Spawning of *Lytechinus pictus* was induced by intracoelomic injection of 0.55 M KCl. The eggs were washed, fertilized with a dilute sperm suspension, cultured at 15°C in filtered sea water (FSW), and staged according to Lane et al. (1993).

Embryos were prepared for microscopy by placing them in viewing chambers constructed from Nitex (Tetko Inc., Briarcliff Manor, NY) in a manner similar to the microaquaria fashioned by Gustafson and Kinnander (1956). Embryos sealed into Nitex cages by a coverslip edged with silicone grease can develop to the pluteus stage (L. D. unpublished results). For digitization of the model's initial geometry, chambers were placed on a 15°C stage and viewed in a Nikon Diaphot inverted microscope equipped with DIC optics. An embryo at the mesenchyme blastula stage was optically sectioned and the image was recorded on a Panasonic TQ-2028F optical memory disk recorder using a Dage 72 CCD video camera. This image was digitized using an Image One video image processor (Universal Imaging, Media, PA). The initial geometry of the model embryo was based on a single embryo and scaled to a diameter of 110 μm.

Construction of a finite element template

The finite element simulations in this paper employ a common representation of the three dimensional shape of the late mesenchyme blastula based on the measurements described above. We use this template during simulations of all five of the proposed mechanisms of invagination, and evaluate the success of each mechanism in generating an invagination when we assign different elastic material properties to the components of the embryo. This model template comprises all of the passive elastic structures in the embryo which resist forces of invagination, such as cytoskeletal and extracellular fibers. This simplification allows us to compare the effect of each proposed force-generating mechanism on model embryos of identical design.

Before building the model we must address three questions about the construction of the mesenchyme blastula: (i) how do we represent the geometry of the mesenchyme blastula? (ii) what values of elastic material properties do we use for the model epithelial sheet? and (iii) how do we represent cell- and ECM-generated forces in the five mechanisms we are testing?

Geometry of the template and ultrastructure of the mesenchyme blastula

The late mesenchyme blastula (Fig. 1) is a closed, monolayered, epithelial ball surrounding the blastocoel, which contains loosely organized ECM and primary mesenchyme cells. The epithelial cells vary in shape from cuboidal in the lateral wall of the blastocoel to columnar at the animal and vegetal poles (Dan and Okazaki, 1956). The basal end of the cell monolayer is lined by a thin basal lamina everywhere except at the vegetal plate (Ettensohn, 1984b). The apical ends of all epithelial cells adhere to the apical ECM, which faces the surrounding sea water. The apical ECM consists of two morphologically distinct layers (respectively the 'inner' and 'outer' zone of Spiegel et al., 1989): (i) the apical lamina lies closest to the apical ends of the cells, and (ii) the hyaline layer separates the apical lamina from the sea water.

The morphology of the finite element model is based on the morphology of *Lytechinus pictus* embryos at the mesenchyme blastula stage. We have modeled only the vegetal half of the mesenchyme blastula (Fig. 2A), since microdissection experiments have demonstrated that neither an intact blastocoel nor the animal half of the embryo are needed for invagination (Moore and Burt, 1939;

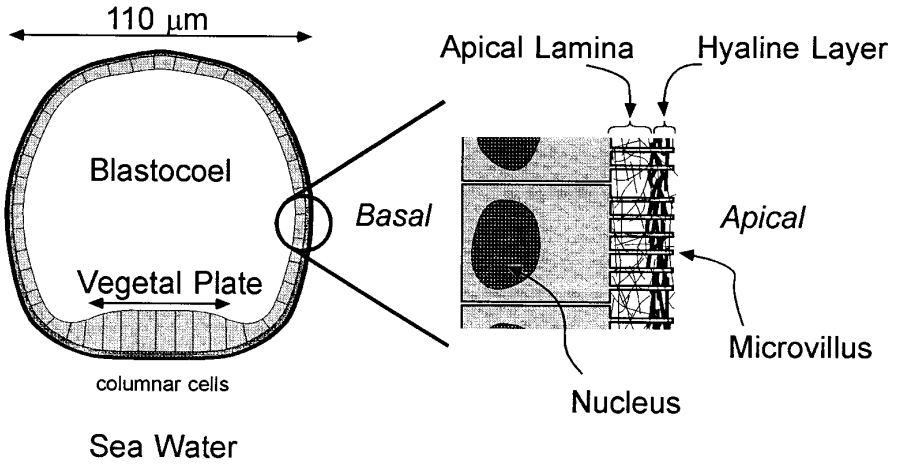

Fig. 1. The ultrastructure of the late mesenchyme blastula of *L. pictus*. The enlargement shows a schematic of the tri-layer sandwich consisting of the epithelial cells, the apical lamina, and the hyaline layer.

Ettensohn, 1984b). Following the observations by transmission electron microscopy (TEM) of discrete layers within the epithelial sheet of *Lytechinus pictus* embryos (Spiegel et al., 1989), we represented the epithelial sheet by three distinct layers: (i) a hyaline layer that is a 1 μm thick, single finite element layer; (ii) an apical lamina that is a 1 μm thick, single finite element layer, and (iii) a cell layer making up the remaining thickness of the sheet, divided into two finite element layers.

Elastic material properties for the template

The values for morphological and mechanical parameters that we used in the construction of our finite element models are listed in Table 2. The details of how we simulated swelling gels, cell protrusions, and contractile bundles for each of the five invagination mechanisms are described below.

The mechanical properties of the sea urchin epithelial sheet from the blastula stage and beyond have not yet been determined. There have been few estimates of the modulii of any epithelial sheet (Tanner et al., 1983). Suction of cells into micropipettes estimate a range of equilibrium modulii from 10 to 135 Pa (1 Pascal = 1 N/m^2 = 1 $pN/\mu m^2$) for the cortex in neutrophils and endothelial cells (Sato et al., 1987; Sato et al., 1990; Hochmuth, 1993). Micropipette and parallel plate compression techniques estimate Young's modulus for the cortex of sea urchin eggs at 120 to 400 Pa (Hiramoto, 1963). These values are similar to the low frequency dynamic modulii of purified cytoskeletal components such as actin gels (300 Pa), microtubule lattices (30 Pa), and vimentin filament lattices (30 Pa; Janmey et al., 1991). The similarity is more than just coincidence, as treatment of endothelial cells with cytochalasin B reduces the modulus of the endothelial cell cortex by a factor of 10 (Sato et al., 1990). Thus, with the consensus that the elastic properties of whole cells arise mostly from the cytoskeleton (Elson, 1988), we have assigned the cell layer a Young's modulus of 20 Pa.

Since the elastic modulii of both the apical lamina and the hyaline layer are unknown, we chose our values with the aim of bracketing the actual ones. A lower limit of 10-20 Pa corresponds to the elastic modulus of tracheal mucus, an ECM made up of concentrated glycosaminoglycans (Seybold et al., 1990). For the upper limit we chose an elastic modulus of sea anenome mesoglea, a matrix that represents a more ordered mixture of collagen and proteoglycans, which is nearly three orders of magnitude stiffer than mucus (Gosline, 1971). The elastic modulii of the apical lamina was varied from 10 to 500 Pa, and that of the hyaline layer from 20 to 4400 Pa. We used a lower range of modulii for the apical lamina because it has thinner and fewer filaments than the hyaline layer, as revealed by high voltage TEM (Spiegel et al., 1989). Although extraordinary elastic modulii (more than 100 MPa) have been measured in other ECM-dominated tissues, these values are derived mainly from highly organized collagen sheets

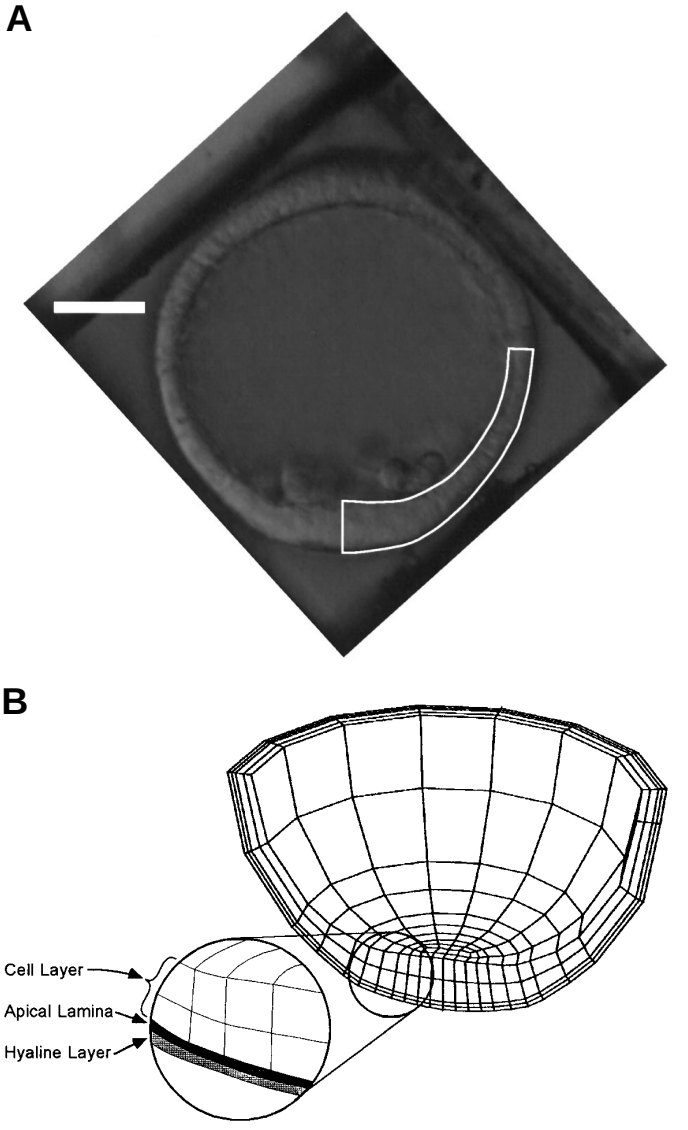

Fig. 2. (A) A mid-sagittal optical section of an *L. pictus* embryo at the mesenchyme blastula stage. (scale bar, 25 μm). The geometry of the finite element model was obtained by digitizing an optical section (outlined in white). (B) A three dimensional view of the finite element model cut mid-sagittally. The cell layer has been divided into a double layer of finite elements.

Table 2. Model parameters used in constructing the finite element simulations

	Model property	Value (range)
(a) Common features	Diameter of embryo	110 μm
	Cell layer elastic modulus	20 Pa
	Apical lamina elastic modulus	(10 to 500 Pa)
	Hyaline layer elastic modulus	(20 to 4400 Pa)
	Apical lamina thickness	1 μm
	Hyaline layer thickness	1 μm
(b) Force generating attributes		
Apical constriction	Diameter of constricting region	42 μm
	Initial strain at the apical face	+0.5
	Initial strain at the basal face	–0.5
Cell tractor	Diameter of anchoring region for contractile protrusions	42 μm
	Length of protrusions	4 μm
	Cross-sectional area of contractile protrusions	1 μm^2
	Stiffness of of contractile protrusions	100 000 Pa
	Initial strain of protrusion	+0.5
Apical contractile ring	Diameter of contractile annulus	42 μm
	Cross-sectional area of annulus	1 μm^2
	Stiffness of annulus	7500 Pa
	Initial strain of annulus	+0.35
Apico-basal contraction	Diameter of contracting region	42 μm
	Cross-sectional area of contractile elements	1 μm^2
	Stiffness of contractile elements	30 000 Pa
	Initial strain of contractile elements	+0.5
Gel swelling	Diameter of swelling region	34 μm
	Initial strain of apical lamina	–0.5

(Fithian et al., 1990); the absence of such organized sheets from the sea urchin ECM allowed us to impose an upper limit well below these values.

Force-generating mechanisms within the template

There have been no measurements of the forces generated by epithelial cells in the sea urchin late mesenchyme blastula. Waddington (1939) made one of the few measurements of stress generated within embryonic tissues, finding that migrating mesoderm in the gastrulating newt *Triton alpestris* generated 3-4 Pa. Reconstituted endothelial cell/tissue culture systems can generate stresses of 10000 Pa (Kolodney and Wysolmerski, 1992). In contrast, swelling granules of ECM secreted by mast cells generate pressures of about 10^6 Pa (Nanavati and Fernandez, 1993). Measurements of forces generated by single cell processes or cytoskeletal structures are also rare, but include the contractile ring of cleaving sand dollar eggs at 0.016 μN force (Rappaport, 1977), axons of PC-12 neurites at 0.4 μN (Lamoureux et al., 1992), and fibroblasts contracting a collagen gel at 0.1 μN (Kolodney and Wysolmerski, 1992).

In our finite element models, we used values of pressures and forces from within these ranges to simulate the forces generated both by cells and ECM. We have used the isotropic expansion of a 3-D solid to mimic the swelling of the ECM layer and the isotropic shrinkage of a 3-D solid to simulate constriction of the subcortical microfilament gel within cells. Shrinkage of 1-D rods mimic the contraction of cell protrusions driving the cell tractoring mechanism. Actively tractoring cells send out protrusions, which attach to prospective substrata, and then contract, thereby pulling the cell body after it. The rods in our model represent cell protrusions only during the contraction phase, after they have formed. Shrinkage of 1-D rods across the apical face of the cell layer is used to simulate bundles of contractile microfilaments involved in the apical contractile ring mechanism while shrinkage of similar 1-D rods across the cell layer thickness simulate contraction of discrete sub-cortical cytoskeletal structures in the apicobasal contraction mechanism. Both swelling and contracting materials generate forces by imposing an initial strain within the vegetal plate. The overall change in shape of the embryo is due to the response of the passive elastic properties of the epithelial sheet to that initial strain.

RESULTS AND DISCUSSION

The apical constriction model

The apical constriction hypothesis posits that the microfilament network at the apical end of the cells contracts, presumably driven by myosin, so that the apical surface of each cell decreases its projected area. In other systems (see below) this constriction generally throws the apical surface into folds, and forces the cytoplasm along with the cell's internal organelles towards the basal end of the cell. The resulting reduction in the apical surface area and increase in the basal surface area bend the epithelium.

Such morphologic indicators have implicated apical constriction in chick neurulation (Schoenwolf et al., 1988; Ferreira and Hilfer, 1993), amphibian gastrulation (Baker, 1965; Hardin and Keller, 1988) and neurulation (Burnside, 1971; Clausi and Brodland, 1993), *Drosophila* ventral furrow and posterior midgut formation (Sweeton et al., 1991; Costa et al., 1994), optic cup formation (Zwaan and Hendrix, 1973), and a variety of other epithelial morphogenetic events (e.g. Hilfer and Hilfer, 1983). Several other lines of evidence suggest that apical constriction plays a role in epithelial morphogenesis. First, electron microscopy and immunofluorescence reveal bundled microfilaments running circumferentially just within the apical face of cells in actively bending epithelia. While the existence of circumapical microfilaments have implicated apical constriction in newt neurulation (Burnside, 1971), *Drosophila* ventral furrow formation, and posterior midgut invagination (Kiehart, 1990), this evidence is merely 'guilt-by-association', for nearly all epithelial sheets have pronounced circumapical microfilament bundles, whether or not they ever deform. These microfilament bundles typically underlie the junctional complexes of polarized epithelia and are presumed to play a role in the maintenance of this polarity (Gumbiner, 1990). In the sea urchin *Strongylocentrotus purpuratus*, microfilament bundles have been identified by immunofluorescence in vegetal plate cells of the mesenchyme blastula (Anstrom, 1992), as well as by TEMs of cells within the archenteron of the early gastrula (Ettensohn, 1984b).

Stronger evidence for apical constriction comes from microfilament inhibition experiments. Cytochalasin B and D block or inhibit many, but not all, of the coordinated cell shape changes and tissue movements in chick neurulation (Schoenwolf et al., 1988). However, in the sea urchin, cytochalasin B and D disruption of microfilaments during invagination eventually leads to complete dissociation of the cells, but does not impair primary invagination (Ettensohn, 1984a; Lane et al., 1993). Unfortunately, results of cytoskeletal disruption experiments are typically ambiguous because of the difficulty of developing artifact-free microfilament fixation protocols (McDonald and Morphew, 1993) and because functionally distinct classes of microfilaments react differently to drug action (Watts and Howard, 1992).

The mechanical process of apical constriction has been modeled by a variety of methods, and it appears to be a plausible generator of epithelial bending (Jacobson and Gordon, 1976; Odell et al., 1981; Hilfer and Hilfer, 1983; Gordon and Essner, 1987; Dunnett et al., 1991; Clausi and Brodland, 1993).

We implement apical constriction in our simulation by imposing a gradient of constriction along the cell axis; cells contract at their apical face and expand at their basal face so as to maintain a constant cell volume (Fig. 3A). In the simulations, the region of active apical constriction (a circular region roughly 40 μm in diameter centered on the vegetal pole) includes most of the cells of the vegetal plate. The maximum stresses generated in apically constricting cells of the vegetal plate is 10 Pa ({maximum stress generated} = {initial strain} × {modulus of the strained layer}). The cells lateral to this region have the same elastic modulus as the vegetal cells, but do not undergo apical constriction and therefore do not generate any stress.

Our simulations demonstrate that apical constriction can indeed produce gastrulae whose invagination matches that of embryonic shapes (Fig. 3B). The stiffness of the ECM has a strong influence on the behavior of the apical constriction model. Realistic invagination occurs only if the apical ECM layers are as easily deformed (i.e. have a similar elastic modulus) as the cell layers (see Fig. 3C).

The cell tractor model

The cell tractor hypothesis proposes that cells lateral to the vegetal plate pull themselves toward the center of the plate using the apical ECM as a mechanical substratum. This directional crawling generates the compressive forces on the vegetal plate cell sheet that cause it to buckle (Burke et al., 1991).

Characterization of cell shapes, observation of rearrangement within cell sheets, and observation of directional crawling at cell sheet edges have implicated cell tractoring as a force-generating mechanism in other morphogenetic events. Cell rearrangement during amphibian neurulation may be the by-product of cortical tractoring (Jacobson et al., 1986). The morphogenetic movements of wound healing are also strongly dependent on the forces generated by crawling cells. Cells at the very edge of a wound as well as cells a few cell columns away from the wound edge contribute to forces closing the wound (Radice, 1980). Cells appear to tractor during the convergence and extension movements of *Xenopus* gastrulation (Shih and Keller, 1992).

Burke et al. (1991) have made four observations in support of the cell tractor model: (i) cells lateral to the vegetal plate have protrusions directed toward the center of the vegetal plate; (ii) lateral cells have a skewed shape and the apical ends appear to be oriented toward the center of the plate; (iii) cells lateral to the vegetal plate move 4 to 5 cell diameters toward the center of the vegetal plate during the course of primary invagination, and (iv) primary invagination is blocked when embryos are cultured with antibody Fab fragments to glycoprotein substrates localized in the apical ECM, implicating the apical lamina as a substratum for cell tractoring.

We simulate the cell tractor model by appending contractile

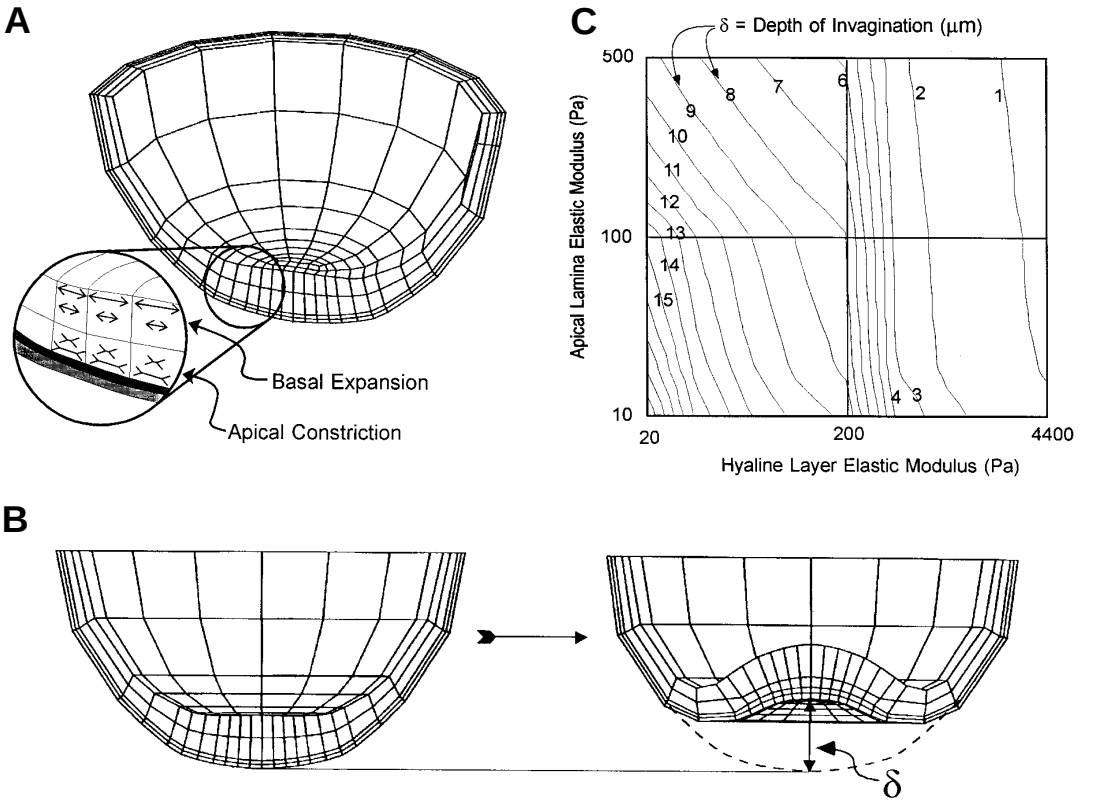

Fig. 3. The apical constriction model. (A) Schematic of the distribution of contractile forces assumed in the model simulations. The arrows indicate the degree of isotropic swelling (arrows directed against the cell membrane) and the degree of isotropic contraction (arrows directed inward from the cell membrane). (B) Initial geometry and final invaginated geometry from a single run of the apical constriction model. The depth of the invagination (δ in μm) used in C is defined as the change in position of the center of the vegetal plate. (C) Invagination (δ) occurring at different values of stiffness (E) of the apical lamina (vertical axis) and the hyaline layer (horizontal axis). The contour lines connect points in this elastic modulus parameter space which generate identical depths (δ) of invagination. The parameter space shown here is a portion of a plane where the cell stiffness is 20 Pa (1 Pascal = 1 N/m^2 = 1 $pN/\mu m^2$), the apical lamina stiffness varies from 10 to 500 Pa, and the hyaline layer stiffness varies from 20 to 4400 Pa. Note that while the scale of the elastic modulii axes are different in each quadrant of C, the material properties are continuous.

protrusions to a ring of cells about 20 μm from the center of the vegetal plate, a region that includes most of the cells that participate in primary invagination. At the start of the simulation, these processes have extended approximately 4 μm. In the real embryo these processes would extend nearly half way across the face of their more vegetal neighboring cells. The proximal end of the process is anchored at the apical face of the cell layer while the distal end extends to the interface between the apical lamina and the hyaline layer (Fig. 4A). Each of the 24 contracting processes are placed at junctions between finite elements surrounding the vegetal plate. Each process can generate a maximum force of 0.025 μN ({maximum force generated by each process} = {initial strain of the process} × {cross sectional area of the process} × {modulus of the process}). The maximum stress developed through the apical lamina is nearly 5000 Pa. Like those processes seen by Burke et al., all of these contractile processes are oriented towards the center of the vegetal plate; their contraction drives the invagination.

Our version of the cell tractor hypothesis generates forces sufficient to buckle the epithelial sheet to the correct geometry, and we find that a wide range of elastic modulii allow for a successful invagination (Fig. 4B,C).

The apical contractile ring model

Although, the cell tractor model of cells tractoring on the apical ECM was proposed to account for the appearance of skewed cells during primary invagination in *Strongylocentrotus purpuratus* (Burke et al., 1991), there are other mechanisms that can both generate the skewed cell shapes and initiate invagination in the mesenchyme blastula. One of these, an apical contractile ring model, is based on the wound healing mechanism observed in epithelia of *Xenopus* embryos (Martin and Lewis, 1992). Cells at the leading edge of this wound form a massive, circumferential microfilament bundle surrounding the wound. Contraction of this cable closes the wound, often leaving a small mound of epithelial cells at the point of closure. In the contractile ring hypothesis proposed here, an annulus of contracting cytoskeletal elements runs through the apical end of a ring of cells encircling the vegetal plate. Unlike wound healing, there is resistance provided by the epithelial sheet within this contractile ring. As this cable contracts it compresses the epithelium at the center of the vegetal plate, causing the vegetal plate to buckle inward.

In our simulations a contractile ring, approximately 40 μm in diameter and centered on the vegetal plate, is installed at the apical face of the cell layer where the cell layer meets the apical lamina (Fig. 5A). This ring generates a maximum contractile force of 0.0032 μN. Contraction of the cable drives both invagination of the plate and coordinated shape changes in the cell layer shown in Fig. 5B. The direction and degree of buckling is determined by the stiffness of the apical lamina and the hyaline layer relative to the cells and the contractile ring (see Fig. 5C).

The apicobasal contraction model

The apicobasal contraction hypothesis proposes that cells of the vegetal plate contract along their apical to basal axis. Like the reduction of cell-cell adhesion proposed in the differential adhesion hypothesis, apicobasal contraction generates compressive forces within the cell layer of the vegetal plate cell sheet that cause the vegetal plate epithelium to buckle inward.

Gustafson and Wolpert (1963) proposed the apicobasal contraction hypothesis as a corollary of the differential adhesion hypothesis to account for two observations: (i) cells in the vegetal plate of the sea urchin *Psammechinus miliaris* decrease their contact areas with each other, and (ii) the basal surface

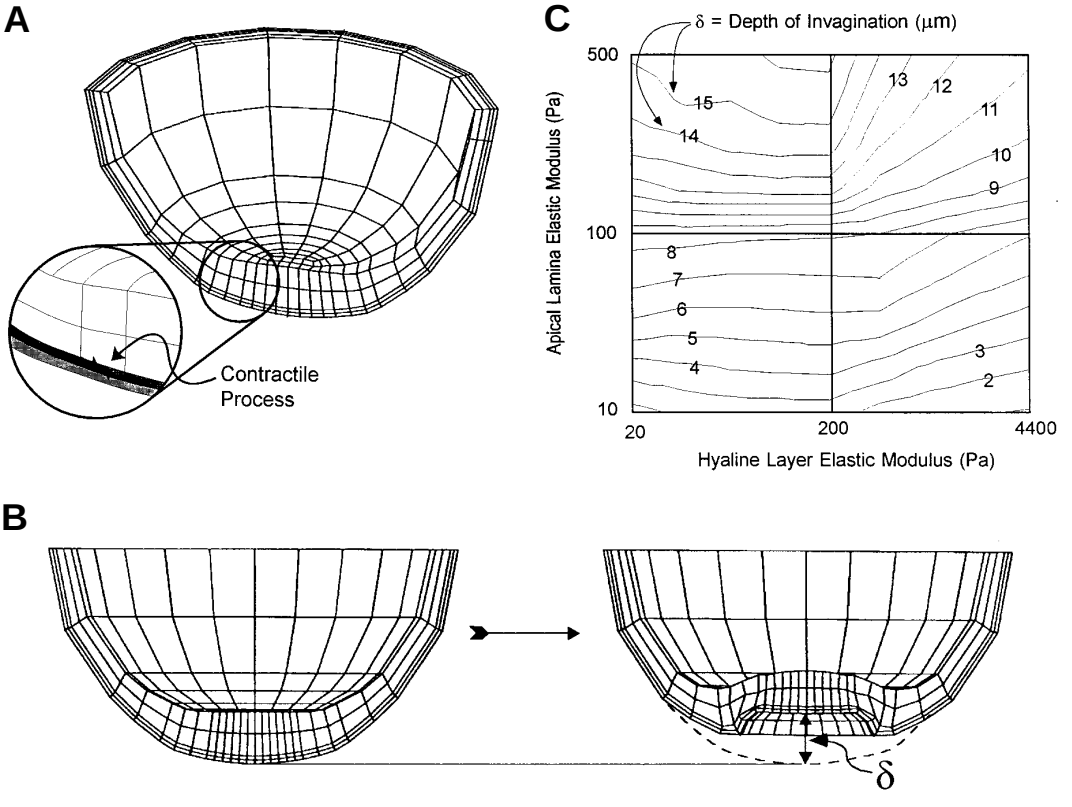

Fig. 4. The cell tractor model. (A) Schematic of the location and direction of the contractile protrusions. (B) Initial geometry and final invaginated geometry from a single run of the cell tractor model. (C) Invagination (δ) occurring at different values of stiffness (E) of the apical lamina (vertical axis) and the hyaline layer (horizontal axis). The contour lines connect points in this elastic modulus parameter space which generate identical depths (δ) of invagination. Note that while the scale of the elastic modulii axes are different in each quadrant of C, the material properties are continuous.

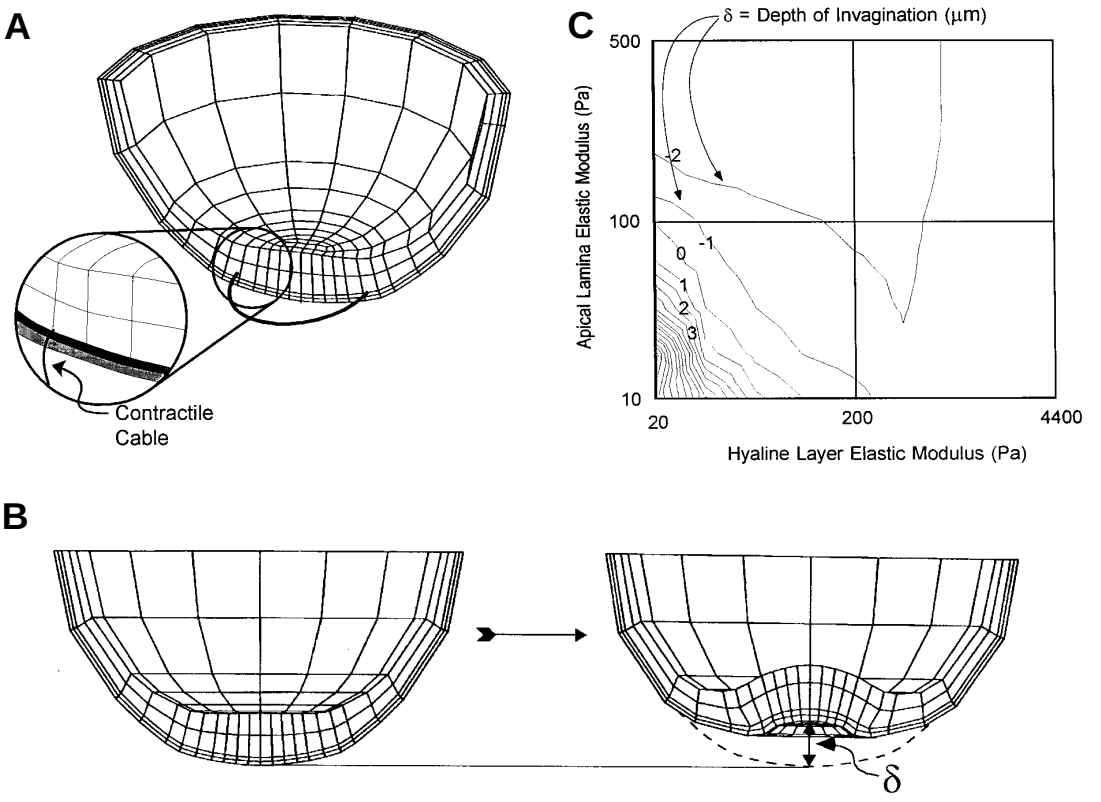

Fig. 5. The apical contractile ring model. (A) Schematic showing the location and orientation of the contractile annulus. (B) Initial and final invaginated geometry of a single run of the apical contractile ring model. (C) Invagination (δ) occurring at different values of stiffness (E) of the apical lamina (vertical axis) and the hyaline layer (horizontal axis). The contour lines connect points in this elastic modulus parameter space which generate identical depths (δ) of invagination. Note that while the scale of the elastic modulii axes are different in each quadrant of C, the material properties are continuous.

of these same cells round and become pulsatory. They noted that such changes in cell shape may be generated by either reductions in cell-cell adhesion between cells of the vegetal plate or by increases in tension directed against the apical and basal faces of these same vegetal plate cells.

Apicobasal contraction has received little attention as a possible motive force driving invagination. The sub-cortical cytoskeleton seems a likely candidate to generate these forces. Both microfilaments and microtubules are present in the sub-cortical cytoskeleton (Hardin, 1987a; Anstrom and Raff, 1988). Microtubules are also found oriented parallel to the apicobasal axis (Hardin, 1987a). Oriented microtubules generate tension responsible for chromosome segregation (Nicklas, 1988) as well as generating tension in PC-12 neurites (Dennerll et al., 1988).

We simulate apicobasal contraction by embedding contractile elements across the thickness of the cell layer within 20 μm from the center of the vegetal plate, a region that includes many of the cells that actively bleb as observed by Gustafson and Wolpert. Nearly a hundred discrete contractile elements extend across the full thickness of the cell sheet connecting the apical surface with the basal surface. These contractile rods are placed at every juncture between finite elements throughout the actively contracting region (Fig. 6A). Each of these contractile rods generates a maximum force of 0.015 μN. The average maximum contractile stress generated is nearly 1200 Pa.

The forces generated by this apicobasal contraction are sufficient to buckle the epithelial sheet to the correct geometry (Fig. 6B). Additionally, we find that a wide variety of elastic modulii allow for a successful invagination (Fig. 6C).

The gel swelling model

The gel swelling hypothesis of Lane et al. (1993) proposes that cells in the vegetal plate secrete a hydrophilic proteoglycan into the apical lamina of the late mesenchyme blastula. As the condensed granules are secreted they swell, analogous to the swelling of mucin granules after exocytosis from goblet cells (Verdugo, 1990), or the swelling of heparin gels following mast cell degranulation (Fernandez et al., 1991). This differential swelling of the apical lamina relative to the non-swelling hyaline layer creates a bending moment throughout the vegetal plate that buckles the vegetal plate inward (Fig. 7A).

Gel swelling has been invoked as a motive force in epithelial morphogenesis in several settings. For example, notochord straightening of tailbud stage *Xenopus* embryos also appears to be dependent on interactions between the stiffening of an ECM sheath and the swelling of vacuoles in the cells of the notochord (Adams et al., 1990; Koehl et al., 1990). Similarly, during the formation of the mouse otic vesicle (Haddon and Lewis, 1991), the secretion of an extracellular bolus of hyaluronic acid swells and pushes the epithelium inward. In the sea urchin, however, the apical ECM invaginates with the rest of the vegetal plate (Citkowitz, 1971; Adelson and Humphreys, 1988; Lane et al., 1993), making it impossible for gel swelling to force the epithelium aside as it does in the developing otic vesicle.

Lane et al. (1993) have made several observations that are consistent with the gel swelling hypothesis: (i) a chondroitin sulfate proteoglycan is secreted into the apical ECM as the vegetal plate buckles to form the early archenteron; (ii) blocking secretion with monensin blocks invagination; (iii) invagination can be stimulated prematurely by introducing a calcium ionophore, A23187, which stimulates the secretion of the proteoglycan; (iv) blocking the secretory pathway with monensin prevents the stimulation of precocious invagination by A23187.

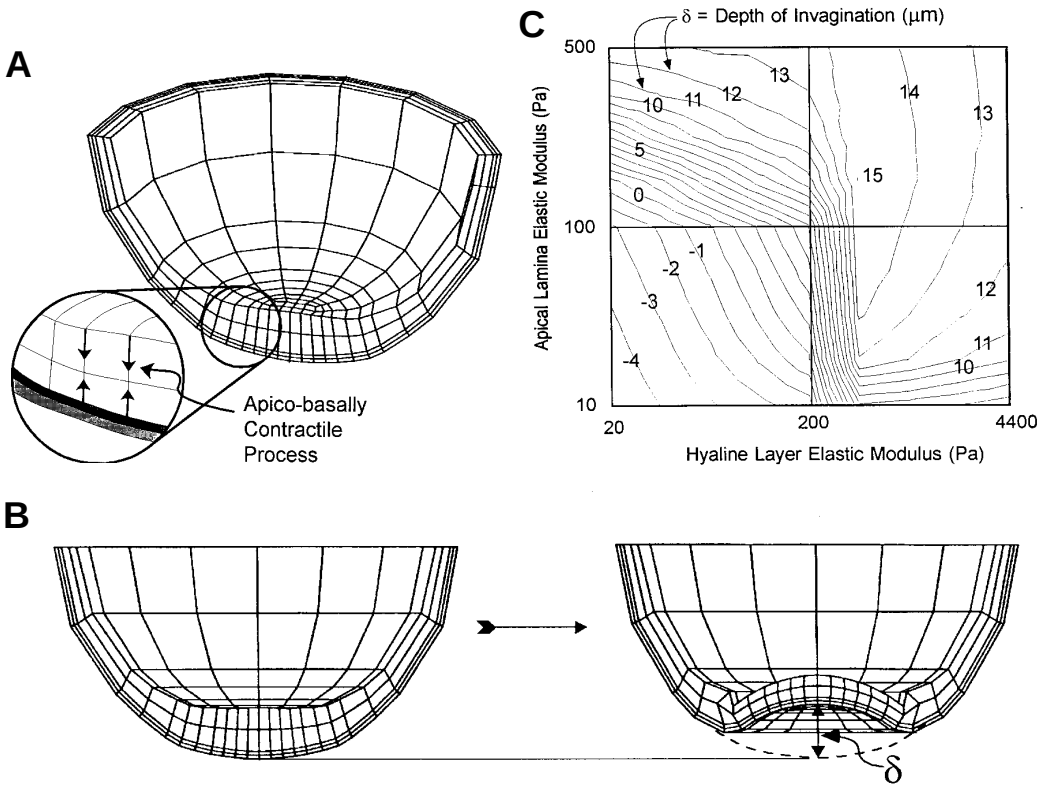

Fig. 6. The apicobasal contraction model. (A) Schematic of the distribution of contractile elements assumed in the model simulations. The arrows indicate the direction of tension directed against the cell membrane. (B) Initial geometry and final invaginated geometry from a single run of the apicobasal contraction model. (C) Invagination (δ) occurring at different values of stiffness of the apical lamina (vertical axis) and the hyaline layer (horizontal axis). The contour lines connect points in this elastic modulus parameter space which generate identical depths (δ) of invagination. Note that while the scale of the elastic modulii axes are different in each quadrant of C, the material properties are continuous.

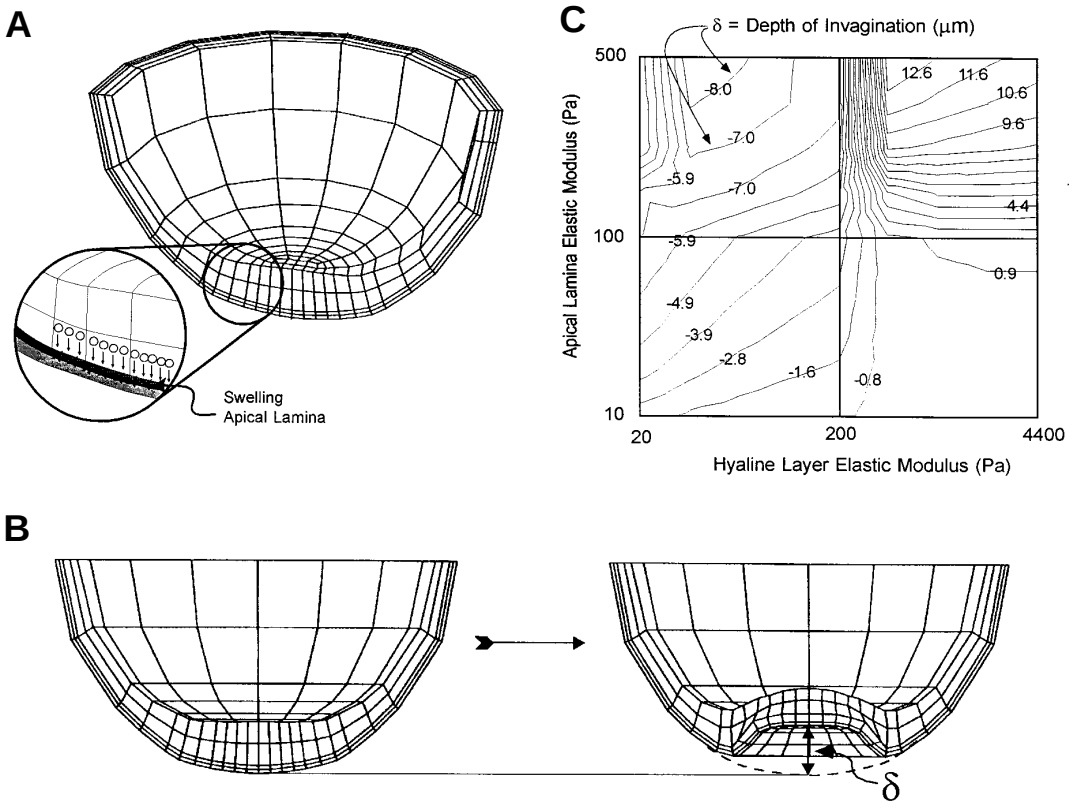

Fig. 7. The gel swelling model. (A) Schematic of the location of cells secreting proteoglycan polymers which form the hydrating polyelectrolyte gel. Initial geometry and final invaginated geometry of a single run of the gel swelling model. (C) Invagination (δ) occurring at different values of stiffness (E) of the apical lamina (vertical axis) and the hyaline layer (horizontal axis). The contour lines connect points in this elastic modulus parameter space which generate identical depths (δ) of invagination. Note that while the scale of the elastic modulii axes are different in each quadrant of C, the material properties are continuous.

In our simulation of the gel swelling hypothesis, the vegetal plate apical lamina covers the region which normally invaginates (approximately 30 μm in diameter centered on the vegetal plate), and swells isotropically. The apical lamina of the surrounding epithelial sheet has the same elastic properties as the apical lamina outside this region, but it does not swell. Constrained by the surrounding epithelium, the vegetal plate buckles inwards as the apical lamina expands (Fig. 7B). The

maximum compressive stresses generated in the swelling gel of the apical lamina varies from 5 to 250 Pa (depending on the stiffness of the apical lamina). The depth of the invagination depends on the stiffness of the expanding apical lamina and the resistance provided by the hyaline and cell layers (Fig. 7C). In order to generate a realistic invagination, the elastic modulus of the cell layer must be significantly lower than those of the ECM layers. Moreover, the apical lamina must be more deformable than the more distal hyaline layer.

Comparison of models

We have translated five hypotheses for primary invagination into mechanical models, each of which we have simulated numerically. With the right combination of elastic modulii, each model can generate a geometrically correct invagination, thus demonstrating that each mechanism can generate the forces necessary to initiate primary invagination. Although the actual cause(s) of primary invagination must be determined experimentally, these simulations identify parameters that could be measured to distinguish between different hypothesized mechanisms: (i) the relative elastic modulii of the cell layer, apical lamina, and hyaline layer required for each mechanism to work, and (ii) the cell shape changes predicted by each hypothesis.

As shown in Fig. 8A, *each mechanism operates within a specific range of mechanical parameters*. For example, creation of a realistic invagination by the apical constriction mechanism requires that the apical lamina be no more than 13 times as stiff as the cell layer and that the hyaline layer be no more than 5 times as stiff, while a similar invagination generated by gel swelling requires that the hyaline layer be at least 60 times stiffer than the cell layer. Similarly, if the forces generated by the apical constriction mechanism are placed within a design whose relative elastic modulii are appropriate to the gel swelling mechanism, apical constriction does not generate an invagination. Fig. 8B-D illustrates the results of simulations done at three points within a range of modulii for the apical lamina and the hyaline layer, holding the elastic modulus of the cell layer constant. At point **I**, the stiffnesses of the cells, apical lamina, and hyaline layer are such that the cell tractor, apicobasal contraction, and gel swelling mechanisms produce invaginations similar in depth to those of early gastrulae (see Fig. 8B). The stiffnesses of the three layers at point **II** permit both the cell tractoring and the apical constriction mechanisms to initiate invagination (Fig. 8C). In contrast, both the gel swelling and apical contractile ring mechanisms generate evaginations at point **II**. The stiffnesses at point **III** allow both the apical constriction and apical contractile ring mechanisms to buckle the vegetal plate inward (Fig. 8D). At each of these points (**I**, **II**, or **III**) some mechanisms are capable of driving invagination, while others fail.

The quantitative results of the contour maps (Figs 3B, 4B, 5B, 6B and 7B) have been extended to include a broader range of elastic modulii for the cell layer. Because our initial choice of 20 Pa for the elastic modulus of the cell layer is not unique (see Constructing a Finite Element Template), we performed additional simulations to explore the role of the cell layer stiffness for each of the mechanisms by allowing the cell layer stiffness to vary from 10 to 1000 Pa. With a stiffened cell layer only the apical constriction mechanism generated a deeper invagination, the others produced negligible invaginations. However, with all mechanisms, if the stiffness of the ECM layers and contractile processes are increased by the same factor as the cell layer stiffness, the calculated depth of invagination turns out to be exactly the same as it had been before any scaling. Thus, the contour map for each hypothesis represents the depth of invaginations for a range of ECM elastic modulii *relative* to the cell layer stiffness.

Shape changes within the cell layer of the vegetal plate over the course of the initial movements of invagination can also be used to discriminate between mechanisms. Differences in the pattern of deformations generated by each mechanism are illustrated in Fig. 9. Each mechanism driving the invagination affects the following aspects of epithelial cell shape in at least four ways: (i) apical skewing, i.e. movement of the apical end of the cell toward or away from the center of the vegetal plate; (ii) apical narrowing, i.e. the change in the width of the apical end of the cell along the vegetal-animal axis; (iii) cell height changes, and (iv) changes in the thickness of the ECM. While cell shapes during invagination have been characterized (Ettensohn, 1984a; Burke et al., 1991), the wide variety of cell shapes present within the invaginating vegetal plate have made the determination of cell shape *changes* impossible from fixed samples since one cannot follow individual cells. However, confocal microscopy of living embryos should enable us to quantify the shape changes of individual cells during primary invagination, and identify those mechanisms that might be generating them.

CONCLUSIONS

Cellular and ECM force-generating processes acting within the embryo's mechanical design drive invagination. The success of a force-generating mechanism in producing an invagination is strongly dependent on geometry and the relative elastic modulii of the cells, and ECM layers. Mechanical simulations allow us to explore this interaction of force-generating mechanisms with the mechanical design of the embryo.

Each mechanism requires a different set of elastic material properties

To discriminate between two or more hypothesized mechanisms for primary invagination, mechanical simulations must be performed within the same framework. We have done this for apical constriction, cell tractoring, apical ring contraction, apicobasal contraction, and gel swelling, and have shown that each can generate sizeable invaginations. However, the success of each mechanism depends on the passive stiffness of the cell layer relative to the stiffness of the two ECM layers. The cell tractoring, apicobasal contraction, and gel swelling mechanisms work only when the ECM is very stiff relative to the cell layer. The apical constriction and apical contractile ring mechanisms each work for a more deformable ECM. On the other hand, the apico basal contraction mechanism requires that the apical lamina be considerably stiffer than the cell layer.

How robust are these mechanisms to other factors in the mechanical design?

These simulations have explored the interaction of the embryo's mechanical design with its force generating mechanisms during primary invagination. Each mechanism is robust (i.e. produces a sizeable initial invagination) over a particular range of apical lamina and hyaline layer stiffnesses relative to the cell layer

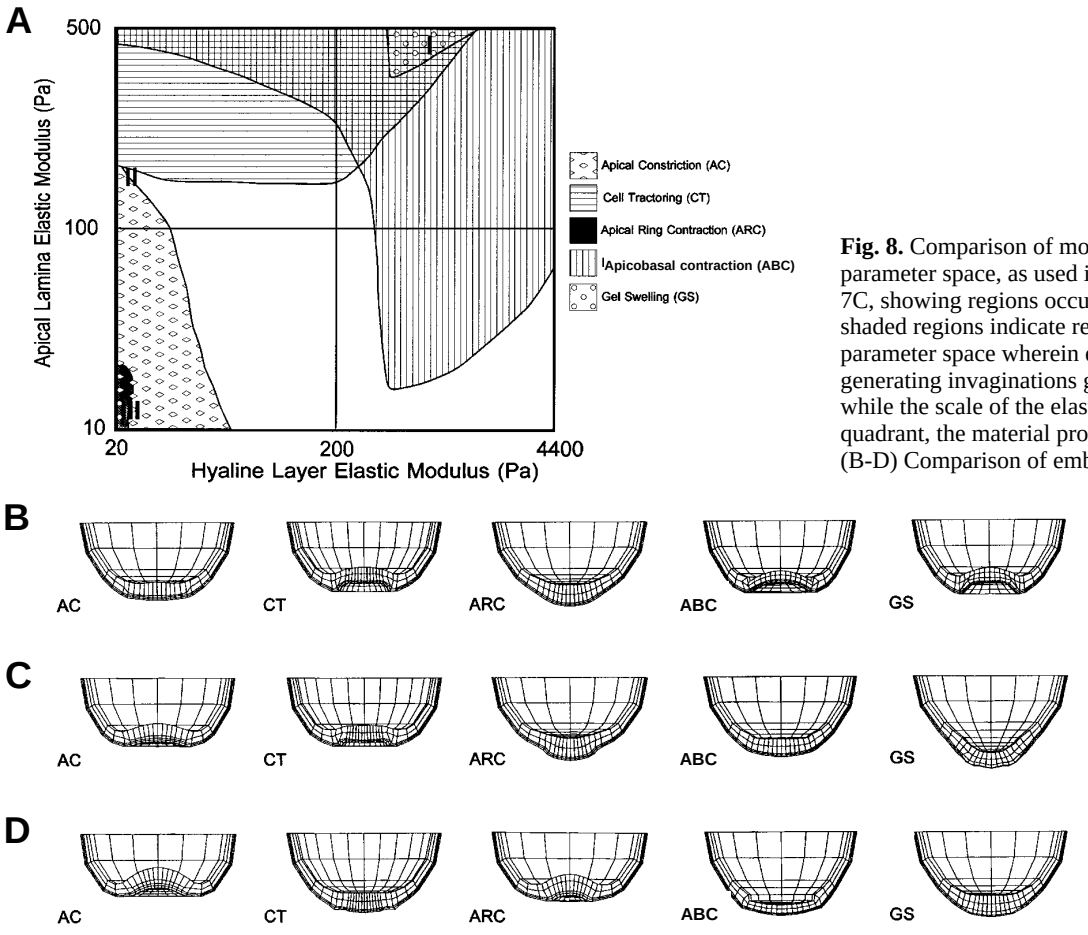

Fig. 8. Comparison of models. (A) The material parameter space, as used in Figs 3C, 4C, 5C, 6C, and 7C, showing regions occupied by the five models. The shaded regions indicate regions of the elastic modulus parameter space wherein each model was capable of generating invaginations greater than 12 μm. Note that while the scale of the elastic modulii change in each quadrant, the material properties are continuous. (B-D) Comparison of embryonic shapes generated by each model at three points in the parameter space. The elastic modulii at these points are: (B at point I) $E_{\text{apical lamina}}$ = 500 Pa, $E_{\text{hyaline layer}}$ = 1250 Pa, E_{cell} = 20 Pa, (C at point II) E_{al} = 200 Pa, E_{hl} = 20 Pa, E_c = 20 Pa, and (D at point III) E_{al} = 10 Pa, E_{hl} = 20 Pa, E_c = 20 Pa. The location of points I, II, and III are indicated in A. (AC, apical constriction; CT, cell tractoring; ARC, apical ring contraction; ABC, apicobasal contraction; GS, gel swelling).

stiffness. Other design features (including the set of parameters listed in Table 2, as well as the overall 3-D geometry) certainly play a role in the results generated by these simulations, but would changes in these parameters invalidate our findings? Our template model can be used as an experimental tool to allow direct determinations of robustness for each parameter.

Simulations predict measurable cell shape changes and mechanical properties

Our simulations suggest experiments that can help to decide which mechanism initiates primary invagination. First, measurements must be made of the elastic modulus of the epithelial sheet and the relative contribution from the cell and ECM layers to that modulus. These simulations demonstrate that each force-generating mechanism requires specific combinations of elastic modulii to generate realistic invaginations. Determinations of these material properties will narrow the field of prospective mechanisms to those that can actually generate an invagination. Second, cell shape *changes* (not just cell shapes) over the course of primary invagination must be characterized. This will further narrow the possibilities to those mechanisms that can produce similar cell shape changes.

It is worth emphasizing that there is a danger in confusing cell shapes with cell shape *changes*. Our simulations calculate the *shape changes* associated with each of these mechanisms. The resulting deformations should only be interpreted after they have been superimposed on the pattern of cell shapes

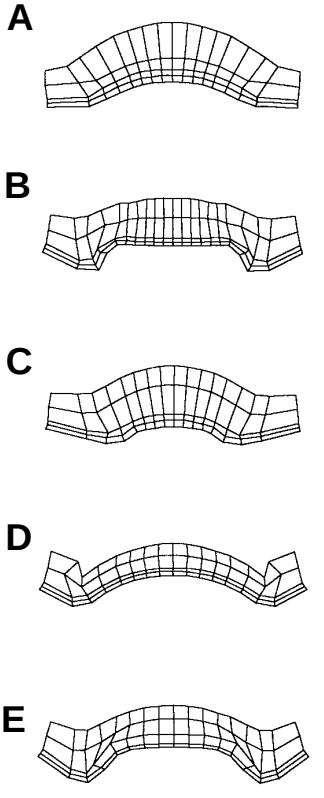

Fig. 9. Shape changes within the vegetal plate. Deformations of the finite elements in a sagittal section of the vegetal plate. The two top layers of finite elements are the cell layer, the bottom layer is the hyaline layer, and the middle layer is the apical lamina. (A) Apical constriction at point I (see Fig. 8A). (B) Cell tractor at point III. (C) Annular ring contraction at point I. (D) Apicobasal contraction at point III. (E) Gel swelling at point III.

present in a real late mesenchyme blastula. This must be done because the cell shapes in the late mesenchyme blastula are not in the least like the purely columnar shapes of the finite elements used to initialize the computer simulations. The skewed cell shapes seen after invagination must be understood as products of forces acting on the already distorted cell shapes present in the late mesenchyme blastula.

Cell shape changes do not require 'smart' cells

Bard (1990) raises the possibility that highly coordinated cell shape changes can drive invagination. This is similar to Jacobson and Gordon's (1976) position on the generation of the neural plate in amphibians, as well as Costa's (1994) proposal for gastrulation in the fly. This view is predicated on the assumption that the complex patterns of cell behaviors and cell shape changes simply mirror the underlying complex pattern of either diffusible morphogens or gene expression. In contrast, each of the simulations detailed here are built on a very simple prepattern (e.g. active cells lie either within or on a prepatterned boundary) and simple behaviors (e.g. cells either contract apically or they do not). Indeed, the complex pattern of cell shape changes seen in our simulations result directly from the interaction of this simple prepatterning with force-generating mechanisms and the passive elastic properties of the embryo.

Identification of mechanical, developmental constraints

Evolutionary shifts from one morphogenetic mechanism to another may require considerable coordination (Oster et al., 1988). The ability to alter one mechanism into another depends on the overlap seen in the Fig. 8A. For example, gradual steps along a *trajectory* through elastic property space do not allow the gel swelling mechanism to change to the apical constriction mechanism because neither mechanism can generate a sufficiently invaginated gastrula with intermediate elastic modulii.

The cellular processes responsible for invagination must take place within the embryo's mechanical design, and that design places strong physical constraints on the course of invagination as well as on evolutionary changes between mechanisms of invagination.

Time, viscosity and the dynamics of primary invagination

The invaginations produced by the above simulations represent equilibrium solutions to the mechanical force balance equations. We have chosen to ignore the time-dependent nature of material properties and forces. Whether a mechanism can drive invagination does not depend on viscoelastic material properties or time-dependent cell behaviors. Invagination in the embryo is dynamic, occurring over several hours. Three of the five hypotheses (apical ring contraction, apicobasal contraction, and gel swelling) exhibit 'snap-through' behavior for certain parameter ranges (Brodland and Cohen, 1987). To investigate their time course we would have to include viscoelastic properties. However, this is not expected to influence the final shape of the invagination.

We still do not know how sea urchins invaginate. But we do know that sea urchins invaginate using forces generated by, and acting on, cells and the ECM. We have begun to understand how invagination might work through a set of comparative mechanical simulations by which we can explore the complex mechanical behavior of the sea urchin embryo. Future biomechanical and morphometric measurements – carried out in conjunction with mechanical simulations – should tell us how invagination works.

We thank Connie Lane and Mike Weliky for insightful suggestions and spirited discussions on morphogenesis, and members of the Keller, Koehl, Oster and Wilt labs for critical comments and reviews. We would also like to thank the anonymous reviewers for suggestions which resulted in the inclusion of the apicobasal contraction model. This work was supported by grants from the NSF to R. E. K. and M. A. R. K. (NSF 92-20525), from the NIH to R. E. K. (HD 25594), from the NSF to G. F. O. (NSF 92-20719), and from the NIH to L. A. D. (5T32GM07379). Special thanks to the MacNeil-Schwendler Corporation for the use of MSC/NASTRANS and MSC/XL.

REFERENCES

Adams, D. S., R. Keller and M. A. Koehl. (1990). The mechanics of notochord elongation, straightening and stiffening in the embryo of *Xenopus laevis*. *Development* **110**, 115-130.

Adelson, D. L. and T. Humphreys. (1988). Sea urchin morphogenesis and cell-hyalin adhesion are perturbed by a monoclonal antibody specific for hyalin. *Development* **104**, 391-402.

Anstrom, J. A. (1992). Microfilaments, cell shape changes, and the formation of primary mesenchyme in sea urchin embryos. *J. Exp. Zool.* **264**, 312-322.

Anstrom, J. A. and R. A. Raff. (1988). Sea urchin primary mesenchyme cells: relation of cell polarity to the epithelial-mesenchymal transformation. *Dev. Biol.* **130**, 57-66.

Baker, P. (1965). Fine structure and morphogenetic movements in the gastrula of the treefrog, *Hyla regilla*. *J. Cell Biol.* **24**, 95-116.

Baker, W. E., P. S. Westine and F. T. Dodge. (1973). *Similarity Methods in Engineering Dynamics*. Rochelle Park, New Jersey: Spartan Books.

Bard, J. (1990). *Morphogenesis*. Cambridge: Cambridge University Press.

Baron, C. J. (1991). *The Structural Mechanics and Morphogenesis of Extant Regular Echinoids Having Rigid Tests.* PhD. Thesis, University of California at Berkeley.

Brodland, G. W. (1994). Finite element methods for developmental biology. *Int. Rev. Cytol.* **150**, 95-118.

Brodland, G. W. and D. A. Clausi. (1994). Embryonic tissue morphogenesis modeled by FEM. *J. Biomech. Eng.* **116**, 146-55.

Brodland, G. W. and H. Cohen. (1987). Deflection and snapping of spherical caps. *Int. J. Solids Struct.* **23**, 1341-56.

Burke, R. D., R. L. Myers, T. L. Sexton and C. Jackson. (1991). Cell movements during the initial phase of gastrulation in the sea urchin embryo. *Dev. Biol.* **146**, 542-57.

Burnside, B. (1971). Microtubules and microfilaments in newt neurulation. *Dev. Biol.* **26**, 416-41.

Butschli, O. (1915). Bemerkungen zur mechanishen erklarung der gastrula-invagination. *Sitzungsberichte Akademie Wissenschaffen, Heidelberg* **4**(B.2), 3-13.

Carter, D. R. (1987). Mechanical loading history and skeletal biology. *J. Biomech.* **20**(11-12), 1095-1109.

Carter, D. R., M. Wong and T. E. Orr. (1991). Musculoskeletal ontogeny, phylogeny, and functional adaptation. *J. Biomech.* **24 Supplement 1**, 3-16.

Cheng, L. Y. (1987a). Deformation analyses in cell and developmental biology. Part I – Formal methodology. *J. Biomech. Eng.* **109**, 10-17.

Cheng, L. Y. (1987b). Deformation analyses in cell and developmental biology. Part II – Mechanical experiments on cells. *J. Biomech. Eng.* **109**, 18-24.

Citkowitz, E. (1971). The hyaline layer: its isolation and role in echinoderm development. *Dev. Biol.* **24**, 348-362.

Clausi, D. A. and G. W. Brodland. (1993). Mechanical evaluation of theories of neurulation using computer simulations. *Development* **118**, 1013-1023.

Costa, M., E. T. Wilson and E. Wieschaus. (1994). A putative cell signal encoded by the folded gastrulation gene coordinates cell shape changes during *Drosophila* gastrulation. *Cell* **76**, 1075-1089.

Dan, K. and K. Okazaki. (1956). Cytoembryological studies of sea urchins. III. Role of the secondary mesenchyme cells in the formation of the primitive gut in sea urchin larvae. *Biol. Bull.* **110,** 29-42.

Dennerll, T. J., H. C. Joshi, V. L. Steel, R. E. Buxbaum and S. R. Heidemann. (1988). Tension and compression in the cytoskeleton of PC-12 neurites. II: Quantitative measurements. *J. Cell Biol.* **107**, 665-674.

Dunnett, D., A. Goodbody and M. Stanisstreet. (1991). Computer modelling of neural tube defects. *Acta Biotheoretica* **39**, 63-79.

Elson, E. L. (1988). Cellular mechanics as an indicator of cytoskeletal structure and function. *Ann. Rev. Biophys. Biophys. Chem.* **17**, 397-430.

Ettensohn, C. A. (1984a). *An Analysis of Invagination During Sea Urchin Gastrulation.* PhD Thesis. Yale University.

Ettensohn, C. A. (1984b). Primary invagination of the vegetal plate during sea urchin gastrulation. *Am. Zool.* **24**, 571-88.

Ettensohn, C. A. (1985). Mechanisms of epithelial invagination. *Q. Rev. Biol.* **60**, 289-307.

Fernandez, J. M., M. Villalon and P. Verdugo. (1991). Reversible condensation of mast cell secretory products in vitro. *Biophys. J.* **59**, 1022-1027.

Ferreira, M. C. and S. R. Hilfer. (1993). Calcium regulation of neural fold formation: visualization of the actin cytoskeleton in living chick embryos. *Dev. Biol.* **159**, 427-440.

Fithian, D. C., M. A. Kelly and V. C. Mow. (1990). Material properties and structure-function relationships in the menisci. *Clin. Orthop. Relat. Res.* **252**, 19-31.

Goodier, J. N. and W. T. Thomson. (1944). *Applicability of Similarity Principles to Structural Models*. National Advisory Committee for Aeronautics, Technical Note, No. 933.

Gordon, S. R. and E. Essner. (1987). Investigations on circumferential microfilament bundles in rat retinal pigment epithelium. *Eur. J. Cell Biol.* **44**, 97-104.

Gosline, J. M. (1971). Connective tissue mechanics of *Metridium senile* I. Structural and compositional aspects. *J. Exp. Biol.* **55**, 763-774.

Gumbiner, B. (1990). Generation and maintenance of epithelial cell polarity. *Cur. Opin. Cell Biol.* **2**, 881-7.

Gustafson, T. and H. Kinnander. (1956). Microaquaria for the time-lapse cinematographic studies of morphogenesis in swimming larvae and observations on sea urchin gastrulation. *Exp. Cell Res.* **11**, 36-51.

Gustafson, T. and L. Wolpert. (1963). The cellular basis of morphogenesis and sea urchin development. *Int. Rev. Cytol.* **15**, 139-214.

Haddon, C. M. and J. H. Lewis. (1991). Hyaluronan as a propellant for epithelial movement: the development of semicircular canals in the inner ear of *Xenopus*. *Development* **112**, 541-550.

Hardin, J. D. (1987a). Archenteron elongation in the sea urchin embryo is a microtubule-independent process. *Dev. Biol.* **121**, 253-262.

Hardin, J. D. (1987b). *The cellular mechanisms and mechanics of archenteron elongation in the sea urchin embryo.* Ph.D. Thesis. University of California.

Hardin, J. (1994). Local cell interactions and control of gastrulation in the sea urchin embryo. *Sem. Dev. Biol.* **5**, 77-84.

Hardin, J. D. and L. Y. Cheng. (1986). The mechanisms and mechanics of archenteron elongation during sea urchin gastrulation. *Dev. Biol.* **115**, 490-501.

Hardin, J. and R. Keller. (1988). The behaviour and function of bottle cells during gastrulation of *Xenopus laevis*. *Development* **103**, 211-230.

Hilfer, S. R. and E. S. Hilfer. (1983). Computer simulation of organogenesis: an approach to the analysis of shape changes in epithelial organs. *Dev. Biol.* **97**, 444-453.

Hiramoto, Y. (1963). Mechanical properties of sea urchin eggs. I. Surface force and elastic modulus of the cell membrane. *Exp. Cell Res.* **32,** 59-xx.

His, W. (1874). *Unsere korperform und das physiologische problem ihrer entstehung*. Leipzig, F. C. W. Vogel.

Hochmuth, R. M. (1993). Measuring the mechanical properties of individual human blood cells. *J. Biomech. Eng.* **115**, 515-519.

Jacobson, A. G. and R. Gordon. (1976). Changes in the shape of the developing vertebrate nervous system analyzed experimentally, mathematically, and by computer simulation. *J. Exp. Zool.* **197**, 191-246.

Jacobson, A. G., G. F. Oster, G. M. Odell and L. Y. Cheng. (1986). Neurulation and the cortical tractor model for epithelial folding. *J. Embryol. Exp. Morphol.* **96**, 19-49.

Janmey, P. A., U. Euteneuer, P. Traub and M. Schliwa. (1991). Viscoelastic properties of vimentin compared with other filamentous biopolymer networks. *J. Cell Biol.* **113**, 155-160.

Kiehart, D. P. (1990). The actin membrane skeleton in *Drosophila* development. *Sem. Cell Biol.* **1**, 325-339.

Koehl, M. A. R. (1990). Biomechanical approaches to morphogenesis. *Sem. Dev. Biol.* **1,** 367-378.

Koehl, M. A. R., D. S. Adams and R. E. Keller. (1990). Mechanical development of the notochord in *Xenopus* early tail-bud embryos. In *Biomechanics of Active Movement and Deformation*. vol. H 42 (ed. by N. Akkas), pp. 471-485. Berlin Heidelberg, Springer-Verlag.

Kolodney, M. S. and R. B. Wysolmerski. (1992). Isometric contraction by fibroblasts and endothelial cells in tissue culture: a quantitative study. *J. Cell Biol.* **117**, 73-82.

Lamoureux, P., J. Zheng, R. E. Buxbaum and S. R. Heidemann. (1992). A cytomechanical investigation of neurite growth on different culture surfaces. *J. Cell Biol.* **118**, 655-661.

Lane, M. C., M. A. R. Koehl, F. Wilt and R. Keller. (1993). The role of regulated secretion of apical extracellular matrix in epithelial invagination in the sea urchin. *Development* **117**, 1049-1060.

Lewis, W. H. (1947). Mechanics of invagination. *Anat. Rec.* **97**, 139-156.

Martin, P. and J. Lewis. (1992). Actin cables and epidermal movement in embryonic wound healing. *Nature* **360**, 179-183.

McDonald, K. and M. K. Morphew. (1993). Improved preservation of ultrastructure in difficult-to-fix organisms by high pressure freezing and freeze substitution: I. *Drosophila melanogaster* and *Strongylocentrotus purpuratus* embryos. *Microsc. Res. Tech.* **24**, 465-473.

Mills, R. (1991). Finite element analysis software. *Computer-Aided Engineering.* **10**, 28-39.

Moore, A. R. (1941). On the mechanics of gastrulation in *Dendraster excentricus*. *J. Exp. Zool.* **87**, 101-111.

Moore, A. R. and A. S. Burt. (1939). On the locus and nature of the forces causing gastrulation in the embryos of *Dendraster excentricus*. *J. Exp. Zool.* **82**, 159-171.

Nanavati, C. and J. M. Fernandez. (1993). The secretory granule matrix: a fast-acting smart polymer. *Science* **259,** 963-965.

Nicklas, R. B. (1988). The forces that move chromosomes in mitosis. *Ann. Rev. Biophys. Biophys. Chem.* **17**, 431-449.

Nislow, C. and J. B. Morrill. (1988). Regionalized cell division during sea urchin gastrulation contributes to archenteron formation and is correlated with the establishment of larval symmetry. *Dev. Growth Differ.* **30**, 483-499.

Odell, G. M., G. Oster, P. Alberch and B. Burnside. (1981). The mechanical basis of morphogenesis. *Dev. Biol.* **85,** 446-462.

Oster, G. F., N. Shubin, J. D. Murray and P. Alberch. (1988). Evolution and morphogenetic rules: The shape of the vertebrate limb in ontogeny and phylogeny. *Evolution* **42**, 862-884.

Radice, G. P. (1980). The spreading of epithelial cells during wound closure in *Xenopus* larvae. *Dev. Biol.* **76**, 26-46.

Rappaport, R. (1977). Tensiometric studies of cytokinesis in cleaving sand dollar eggs. *J. Exp. Zool.* **201**, 375-8.

Rhumbler, L. (1902). Zur mechanik des gastrulationsvorganges insbesondere der invagination. *Arch. Entw. Mech.* **14**, 401-476.

Sato, M., M. J. Levesque and R. M. Nerem. (1987). An application of the micropipette technique to the measurement of the mechanical properties of cultured bovine aortic endothelial cells. *J. Biomech. Eng.* **109**, 27-34.

Sato, M., D. P. Theret, L. T. Wheeler, N. Ohshima and R. M. Nerem. (1990). Application of the micropipette technique to the measurement of cultured porcine aortic endothelial cell viscoelastic properties. *J. Biomech. Eng.* **112**, 263-268.

Schoenwolf, G. C., D. Folsom and A. Moe. (1988). A reexamination of the role of microfilaments in neurulation in the chick embryo. *Anat. Rec.* **220**, 87-102.

Selker, J. M., G. L. Steucek and P. B. Green. (1992). Biophysical mechanisms for morphogenetic progressions at the shoot apex. *Dev. Biol.* **153**, 29-43.

Selman, G. G. (1955). Studies on the forces producing neural closure in amphibia. *Proc. R. Phys. Soc. Edinb.* **24,** 24-27.

Selman, G. G. (1958). The forces producing neural closure in amphibia. *J. Embryol. Exp. Morphol.* **6,** 448-465.

Seybold, Z. V., A. T. Mariassy, D. Stroh, C. S. Kim, H. Gazeroglu and A. Wanner. (1990). Mucociliary interaction in vitro: effects of physiological and inflammatory stimuli. *J. Appl. Physiol.* **68**, 1421-6.

Shih, J. and R. Keller. (1992). Cell motility driving mediolateral intercalation in explants of *Xenopus laevis*. *Development* **116**, 901-914.

Spek, J. (1918). Differenzen im quellungszustand der plasmakolloide als eine ursache der gastrulainvagination, sowie der einstulpungen und faltungen von zellplatten uberhaupt. *Kolloidchemische Beihefte* **9**, 259-399.

Spiegel, E., L. Howard and M. Spiegel. (1989). Extracellular matrix of sea urchin and other marine invertebrate embryos. *J. Morph.* **199**, 71-92.

Stephens, L., J. Hardin, R. Keller and F. Wilt. (1986). The effects of aphidicolin on morphogenesis and differentiation in the sea urchin embryo. *Dev. Biol.* **118**, 64-69.

Sweeton, D., S. Parks, M. Costa and E. Wieschaus. (1991). Gastrulation in

Drosophila: the formation of the ventral furrow and posterior midgut invaginations. *Development* **112**, 775-89.

Tanner, C., D. A. Frambach and D. S. Misfeldt. (1983). Transepithelial transport in cell culture. A theoretical and experimental analysis of the biophysical properties of domes. *Biophys. J.* **43**, 183-190.

Trinkaus, J. P. (1984). *Cells into Organs: The Forces that shape the Embryo.* Englewood Cliffs: Prentice-Hall Inc.

Verdugo, P. (1990). Goblet cells secretion and mucogenesis. *Ann. Rev. Physiol.* **52,** 157-176.

Waddington, C. H. (1939). Order of magnitude of morphogenetic forces. *Nature* **144**, 637.

Waddington, C. H. (1942). Observations on the forces of morphogenesis in the amphibian embryo. *J. Exp. Biol.* **19**, 284-93.

Watts, R. G. and T. H. Howard. (1992). Evidence for a gelsolin-rich, labile F-actin pool in human polymorphonuclear leukocytes. *Cell Mot. Cytoskel.* **21**, 25-37.

Zienkiewicz, O. C. and R. L. Taylor. (1989). *The Finite Element Method: Basic Formulation and Linear Problems*. New York: McGraw-Hill.

Zienkiewicz, O. C. and R. L. Taylor. (1991). *The Finite Element Method: Solid and Fluid Mechanics Dynamics and Non-linearity*. New York: McGraw-Hill.

Zwaan, J. and R. W. Hendrix. (1973). Changes in cell and organ shape during early development of the ocular lens. *Amer. Zool.* **13**, 1039-1049.

(Accepted 3 April 1995)